Chapter 4

Wide-angle Polarization-insensitive Quad-band Metamaterial Absorber

4.1 Introduction

The use of metamaterial/metasurface based absorbers has gained significant attention because of their attractive features like ultrathin and compact structure, low cost, conformal, frequency tunable, and multiband absorption. In the past years, several absorber structures with absorption at single, dual, and triple frequency bands have been proposed [Li *et al.* (2011)a, Lee and Lim (2011), Zhong *et al.* (2012), Dincer *et al.* (2013), Huang *et al.* (2013), Ayop *et al.* (2014)b, Wang *et al.* (2014)b, Ghosh *et al.* (2015), Zhai *et al.* (2015)b, and Lin *et al.* (2015)]. Very few absorber structures [Zheng *et al.* (2013), Mao *et al.* (2014), Chaurasiya *et al.* (2015)] have been reported with quad band and more absorption bands in lower GHz frequency range. This is because of difficulty in achieving absorption in multiple bands due to strict conditions of perfect absorption. A single unit cell consists of 2 x 2 array of split ring resonator (SRR) oriented in different directions was presented by Li *et al.* [Li *et al.* (2010)] to achieve dual-band absorption. In some works, dual/triple band absorption was realized by combining a group of scaled structures in a single unit cell [Li *et al.* (2011)b, Bhattacharyya *et al.* (2013)].

A quad-band polarization-insensitive, wide-angle absorber structure with absorption in C- and X- frequency bands is proposed in this chapter. The proposed unit cell geometry utilizes a 2 x 2 array of the variant of electrical resonator presented in chapter 2 in a single unit cell to achieve quad-band absorption. The proposed absorber is having peak absorption of 98.5 %, 97.7 %, 94.8 % and 96 % at 4.34 GHz, 6.68 GHz,

8.58 GHz, and 10.64 GHz, respectively. The design of the proposed unit cell is presented in section 4.2. The simulated reflection/absorption response of the proposed structure along with the input impedance and constitutive electromagnetic parameters are presented in section 4.3. Parametric analysis is also presented in this section to observe the effect of various shape parameters on the reflection response of the structure. Absorption mechanism of the proposed structure is also discussed with the help of *E*-field and surface current distribution plots in this section. Section 4.4 of the chapter presents the polarization-insensitive and wide-angle performance of the proposed absorber. Experimental verification of the simulated reflection response is presented in section 4.5. Performance comparison of the proposed absorber is presented with other multiband absorbers in section 4.6. Finally, section 4.7 concludes the presented chapter.

4.2 Design of the Unit Cell

The proposed unit cell is a three-layered structure. FR4 dielectric layer ($\varepsilon_r = 4.4, tan\,\delta = 0.02$) is sandwiched between the electric resonator and ground plane made of 35 μm thick copper layers (σ = 5.8 x 10^7 S/m). The thickness of the substrate is 0.8 mm which is a very small fraction of operating wavelength, hence, it is better to treat these structures as metasurfaces. The transmission coefficient of the structure is reduced to zero by utilizing a complete metallic backplane and therefore, the investigation presented in this chapter is focused on the reflective/absorptive properties of the structure.

The unit cell of the proposed absorber structure is simulated using CST Microwave Studio applying periodic boundary conditions. Plane wave modes TE (0, 0) and TM (0, 0) are incident on the structure using Floquet ports. The electric resonator of the proposed unit cell consists of 2 x 2 array of closed ring resonators (CRR). Each CRR

encloses square metallic patches and connected to it diagonally as shown in Figure 4.1. The array elements of a unit cell are oriented perpendicular to each other to achieve four-fold symmetry in the structure. Therefore, the structure becomes polarization insensitive.

The coupling between neighboring unit cells, between CRRs of a unit cell, and between the CRR and the patch alters the electric response of the structure and hence the electric permittivity, ($\varepsilon(\omega)$). The current loops are formed in between the electric resonator and the metallic backplane which adjust the magnetic response and hence the magnetic permeability, ($\mu(\omega)$). The frequency points at which $\varepsilon(\omega)$ and $\mu(\omega)$ are equal has a normalized impedance ($Z = \sqrt{\mu(\omega)/\varepsilon(\omega)}$) of unity. At such frequencies, the impedance of the structure is perfectly matched to that of the free space impedance and hence, the reflectivity ($R(\omega)$) gets minimized which maximizes the absorptivity ($A(\omega) = 1 - R(\omega)$, where $R(\omega) = |S_{11}|^2$) of the structure. The proposed structure is optimized to get near unity absorption in the quad bands. The optimized parameters are: l_s = 20 mm, l_p = 7.7 mm, g_1 = 0.2 mm, w_c = 0.3 mm, and w_d = 0.14 mm.

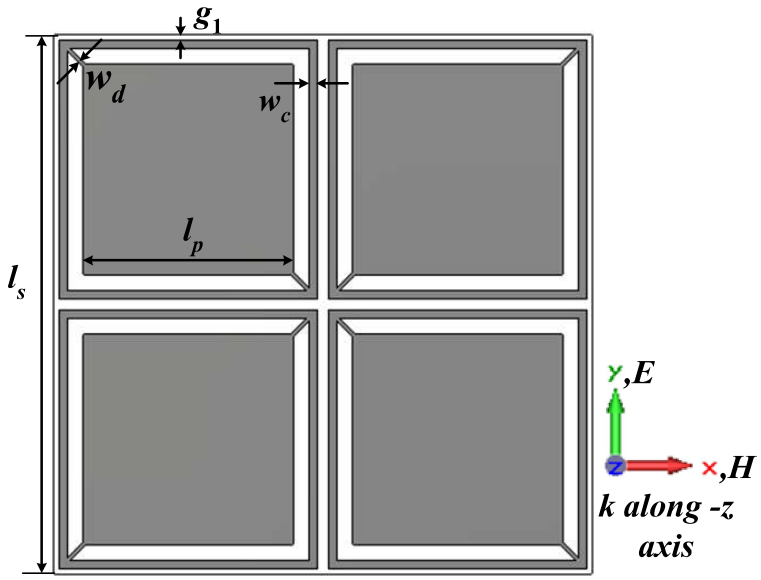

Figure 4.1: Electric resonator of the proposed absorber unit cell.

4.3 Results and Discussion

4.3.1 *S*-parameters

The simulated reflection coefficient characteristics and absorption response of the proposed structure are plotted in Figure 4.2 for the TE and TM polarized normally incident wave. The peak absorption of 98.5 %, 97.7 %, 94.8 %, and 96 % is obtained by the proposed absorber at 4.34 GHz, 6.68 GHz, 8.58 GHz, and 10.64 GHz, respectively. It is observed that the reflection/absorption characteristics of the proposed absorber remain invariant for TE and TM polarized normally incident waves. The full width at half maximum (FWHM) bandwidth of the proposed absorber is 0.17 GHz, 0.27 GHz, 0.40 GHz, and 0.31 GHz in band 1, band 2, band 3, and band 4, respectively.

4.3.2 Normalized Input Impedance

The normalized input impedance (Z) of the proposed structure is calculated using Equation 4.1 and plotted in Figure 4.3. The $Re(Z)$ should be unity and the $Im(Z)$ should have zero transition at the frequencies of absorption. The calculated values of Z at the

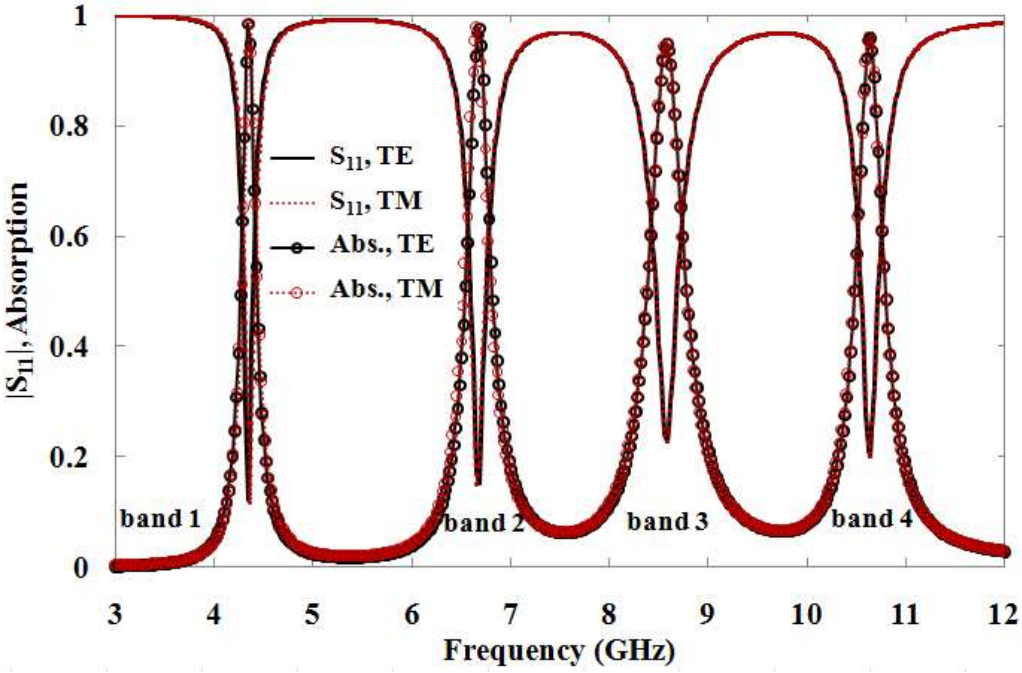

Figure 4.2: Simulated absorption response of the proposed absorber.

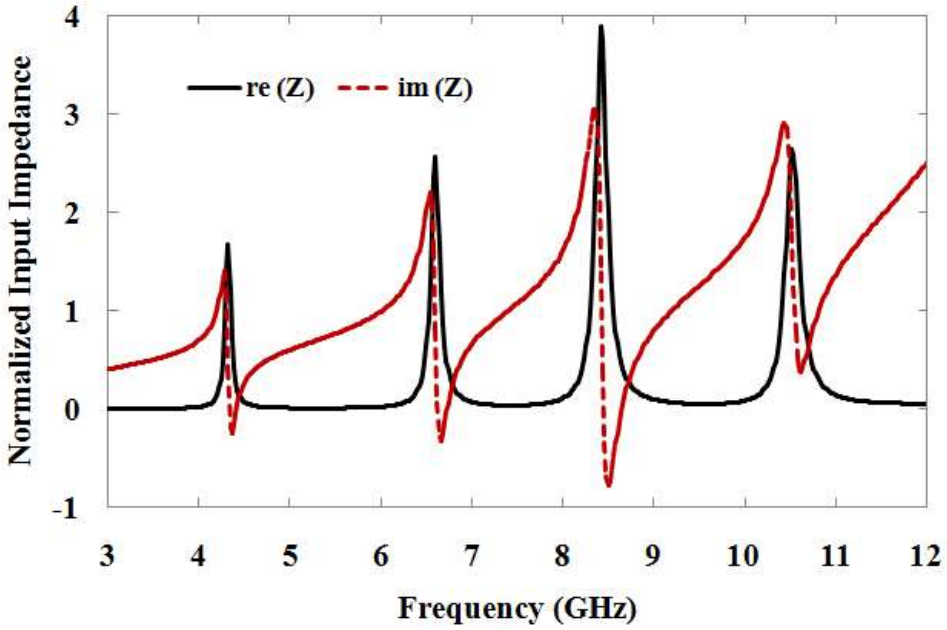

Figure 4.3: Normalized input impedance of the proposed absorber.

peak absorption frequencies of 4.34 GHz, 6.68 GHz, 8.58 GHz, and 10.64 GHz are 1.19−j0.19, 0.86−j0.25, 0.79−j0.36, and 1.08+j0.42, respectively.

$$Z = \sqrt{\frac{\left(1+S_{11}\right)^2 - S_{21}^2}{\left(1-S_{11}\right)^2 - S_{21}^2}} = \frac{1+S_{11}}{1-S_{11}} \tag{4.1}$$

where S_{21} is zero due to the metallic backplane.

4.3.3 Constitutive Parameters (ε_{eff} and μ_{eff})

The constitutive parameters (ε_{eff} and μ_{eff}) of the proposed absorber are calculated using the method provided in chapter 2. For normalized input impedance to be unity (i.e. the condition of perfect absorption), the real part of ε_{eff} and μ_{eff}, and the imaginary part of ε_{eff} and μ_{eff} must be separately equal to each other. The retrieved values at the peak absorption frequencies are presented in Table 4.1. The closeness of the values justifies the attainment of high absorption at these frequencies.

Table 4.1: Retrieved Constitutive Parameters of the Proposed Absorber at the Peak Absorption Frequencies

Frequency	re(ε_{eff})	re(μ_{eff})	im (ε_{eff})	im (μ_{eff})
4.34 GHz	0.64	1.52	2.25	3.28
6.68 GHz	0.44	1.45	1.91	1.54
8.58 GHz	0.34	1.50	1.45	1.10
10.64 GHz	1.35	0.53	0.90	1.21

4.3.4 Parametric Analysis

To observe the effect of the geometrical parameters on the reflection response of the proposed absorber, parametric analysis of some key parameters is performed and presented in Figure 4.4(a)-(c). Only one parameter is changed at a time keeping all other parameters constant. It is observed that all the four resonating frequencies shift towards the lower frequency side by increasing the cell size (see Figure 4.4(a)). It is observed from the resonator geometry that on increasing the l_s, the length of the CRR and diagonal arm increases keeping the length of the patch constant, which in turn increases the associated inductances and thus decreases the resonating frequencies. The variation in l_p (see Figure 4.4(b)) affects the two higher resonating modes only and the resonating frequency decreases with the increase in patch length. It is observed from Figure 4.4(c) that change in the width of the diagonal arm affects the higher most resonating frequency only. The resonating frequency increases with the increase in w_d as the inductance associated with diagonal arm decreases with an increase in its width. It is further noticed that the variation in shape parameters does not affect the reflection and hence absorption level much.

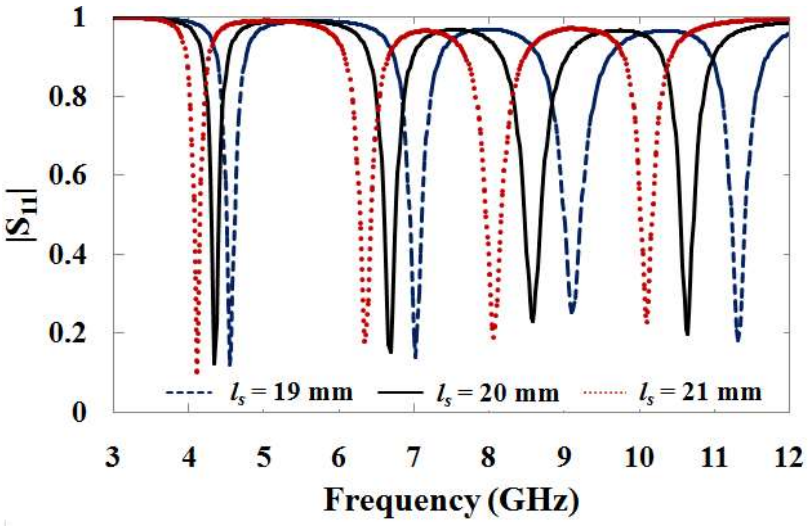

(a)

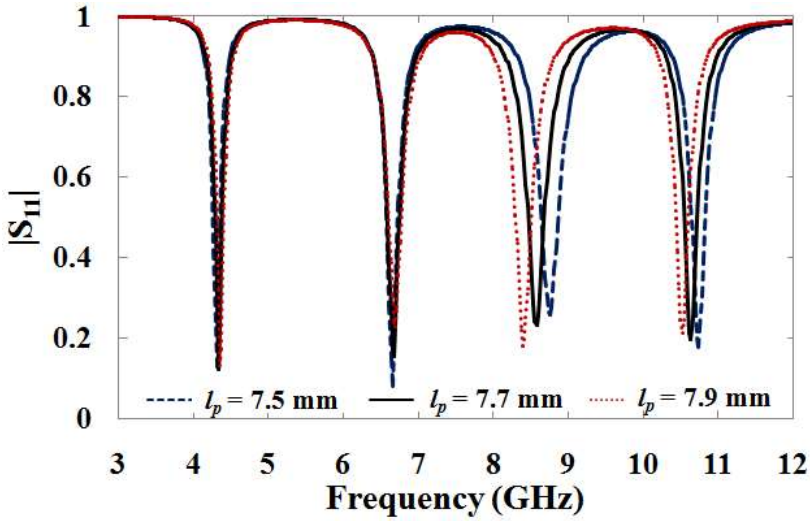

(b)

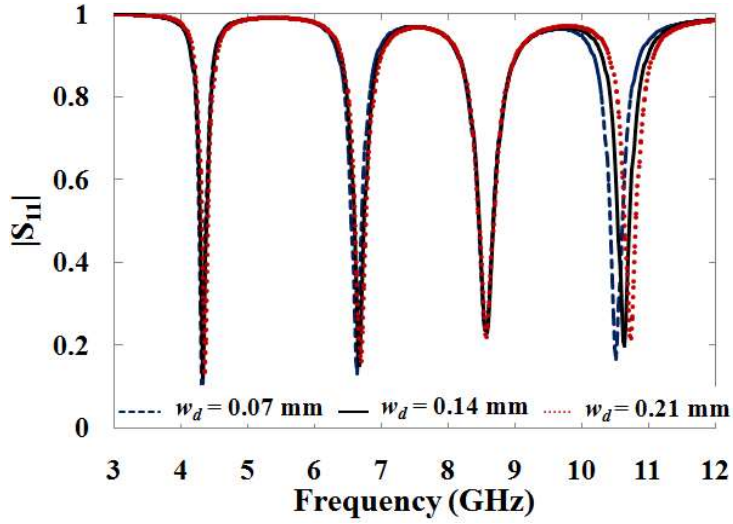

(c)

Figure 4.4: Effect of varying (a) 'l_s', (b) 'lp', (c) 'w_d' on the reflection characteristics.

4.3.5 Power Loss Density and Surface Power Loss Density

The quantitative analysis of power loss density (P_d, representing dielectric losses) and surface power loss density (P_o, representing ohmic losses) at the peak absorption frequencies is presented in Figure 4.5. It is observed that the dielectric loss dominant over the ohmic loss and plays a key role in the absorption phenomenon at the microwave frequencies.

4.3.6 Electric Field and Surface Current

To have an insight into the absorption phenomenon, the electric field and surface current distribution on the proposed absorber is presented in Figure 4.6 and 4.7, respectively for the normally incident TE polarized wave. It is observed from Figure 4.6 that maximum *E*-field is concentrated in the gap between the neighboring unit cells and in the gap between the four CRRs of a unit cell at the first and second absorption frequency, and therefore, most of the power loss takes place in these regions. At the third absorption frequencies, *E*-field is concentrated near the patch corners which are

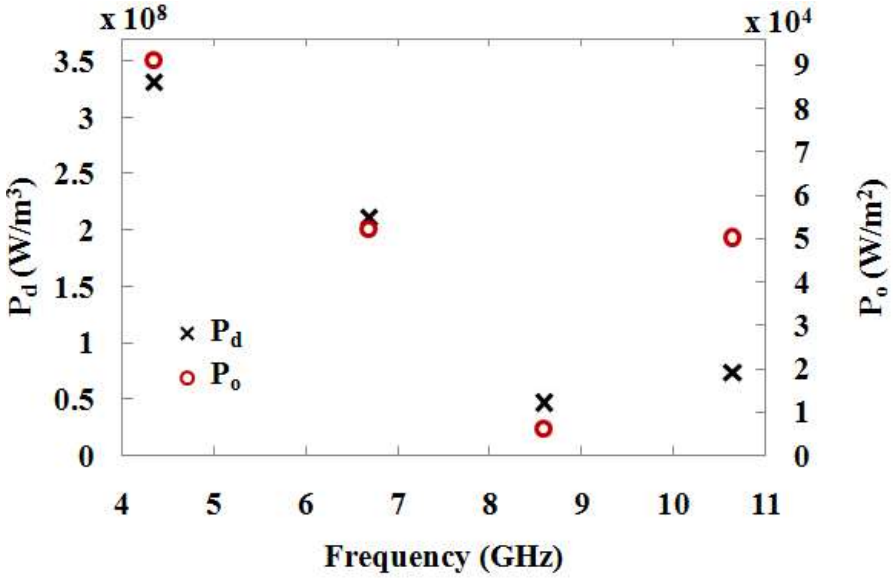

Figure 4.5: Maximum values of dielectric and ohmic losses at the peak absorption frequencies.

disconnected to the CRR. While, for the fourth absorption frequency, the concentration of *E*-field is in the gap between the patch and CRR close to the connected diagonal arms. Figure 4.7 clearly depicts the antiparallel surface current in the top and bottom layers of the absorber at all four frequencies of absorption, and thus current loops are formed which couples the magnetic field perpendicular to it. Therefore, the magnetic resonance is the cause of absorption in the proposed structure.

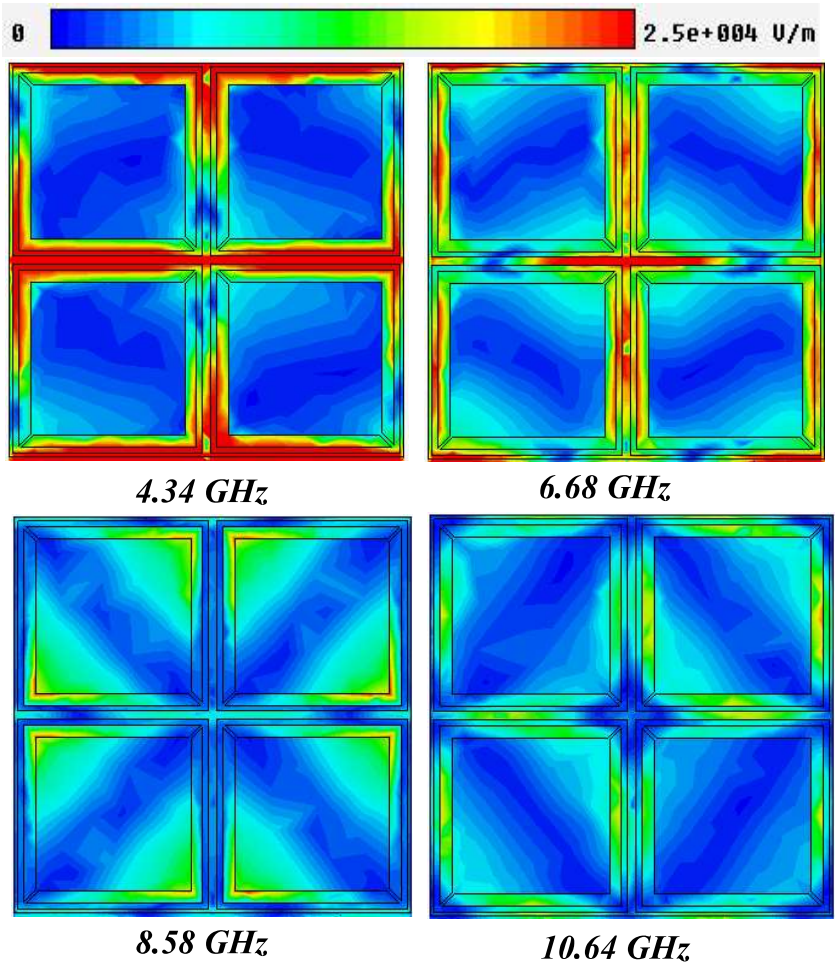

Figure 4.6: Electric field distribution on the proposed structure at the peak absorption frequencies.

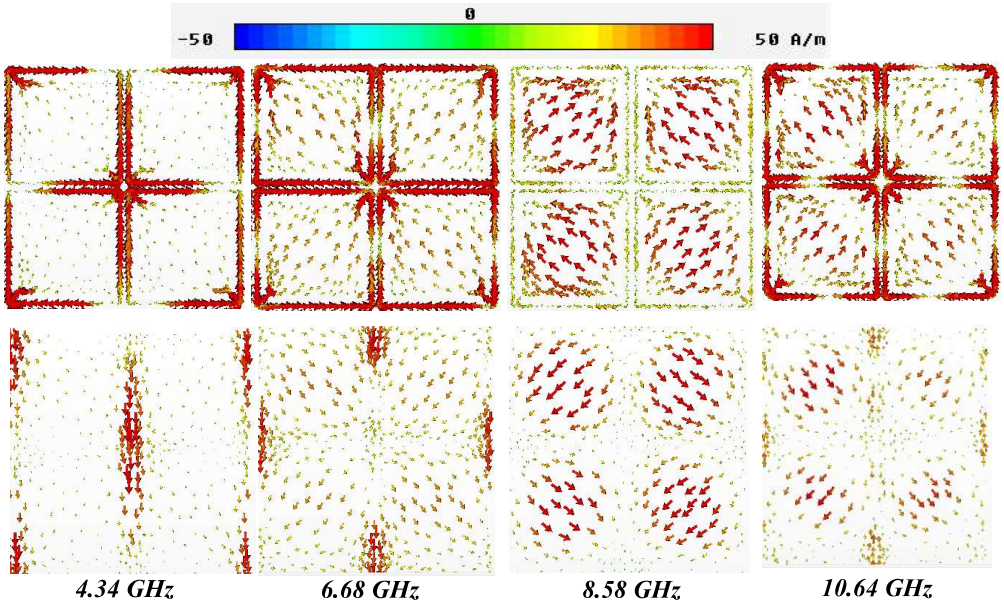

Figure 4.7: Surface current distribution at the resonator and backplane of the proposed structure.

4.4 Polarization-insensitive and Wide-angle Performance

Figure 4.8 shows the polarization insensitive nature of the proposed absorber for a normally incident wave. The variations in angle ϕ rotate the plane containing *E*- and *H*-field vectors. Angle ϕ is varied from 0^0 to 45^0 only, because of diagonal symmetry present in the structure.

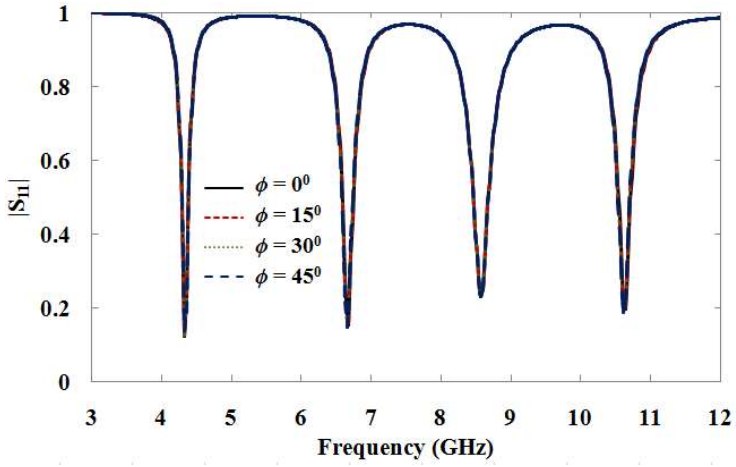

Figure 4.8: Reflection response of the proposed absorber under the variation of polarization angle (ϕ).

Figure 4.9(a) and (b) shows the reflection characteristics of the proposed absorber by varying the angle of incident wave (θ) for TE and TM polarized incident wave, respectively. It is observed that for TE polarized wave, the reflection response remains almost same up to an angle of 60^0 except in band 4. However, for TM polarized incident wave the reflection characteristics remain almost same in all four bands with the generation of some secondary resonances.

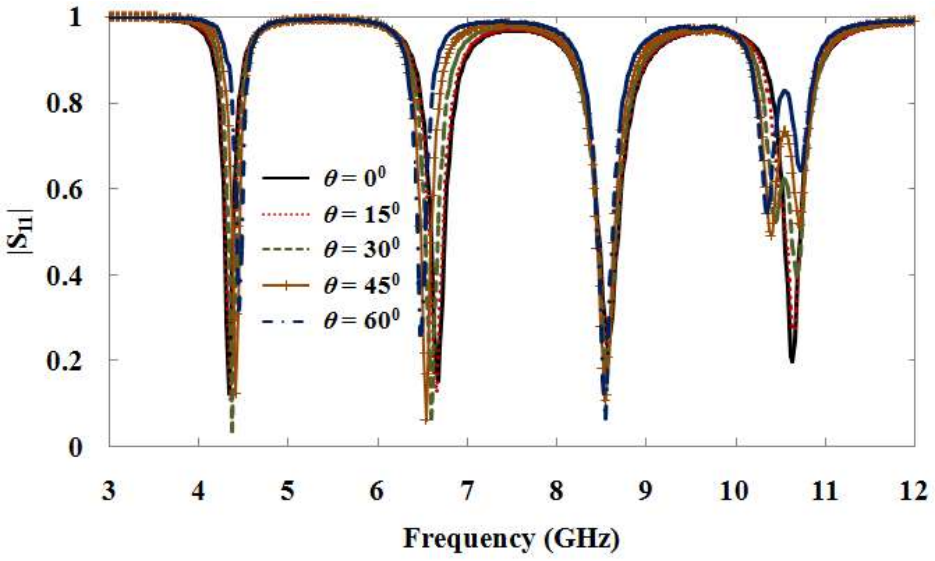

(a)

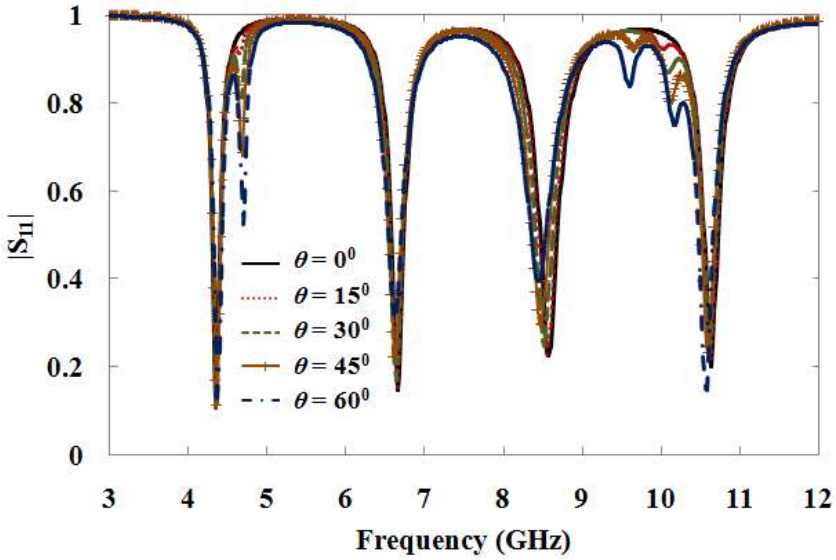

(b)

Figure 4.9: Simulated reflection response of the proposed absorber with the variation of incident angle (θ) for (a) TE polarization and (b) TM polarization.

4.5 Experimental Results

An array of 5 x 5 unit cells of the proposed absorber is fabricated and is shown in Figure 4.10 along with the measurement setup. The fabricated sample is measured using free space measurement method. In this method, a pair of standard horn antennas working in C- and X- bands are used. One antenna is used for transmission and other for receiving the reflected signal from the structure. The two antennas are connected to a vector network analyzer (Anritsu's VNA Master MS2038C). The fabricated sample is placed in front of these antennas in the anechoic chamber in the far field region. Initially, the reflection coefficient is measured by holding a copper sheet of the same dimension as that of fabricated sample. Next, the copper sheet is replaced with the fabricated sample and again the reflection coefficient is noted. Then the actual reflections from the sample can be obtained by normalizing the reflection coefficients of the sample with that of the copper sheet. The simulated and measured reflection characteristics are compared in Figure 4.11. The transmit and receive horn antennas can be put either in TE polarization or TM polarization, as the structure has identical reflection response for both the polarization. The measured peak absorption of 92 %, 99.2 %, 98.7 %, and 90.3 % are obtained at 4.74 GHz, 6.72 GHz, 8.4 GHz, and 10.72 GHz, respectively. The two results are in good agreement; however, the absorption in band 1 is shifted towards higher frequency side. This is due to the small sample size corresponding to the wavelength of peak absorption frequency of the band 1 (4.34 GHz).

4.6 Performance Comparison with Some Other Multiband Absorbers

The proposed absorber is compared with some other quad/pentaband metamaterial absorber in the microwave domain in Table 4.2. It is observed that the proposed

structure is compact and much thinner as compared to the previously reported quad- and pentaband absorber structures.

Figure 4.10: Measurement setup and fabricated sample.

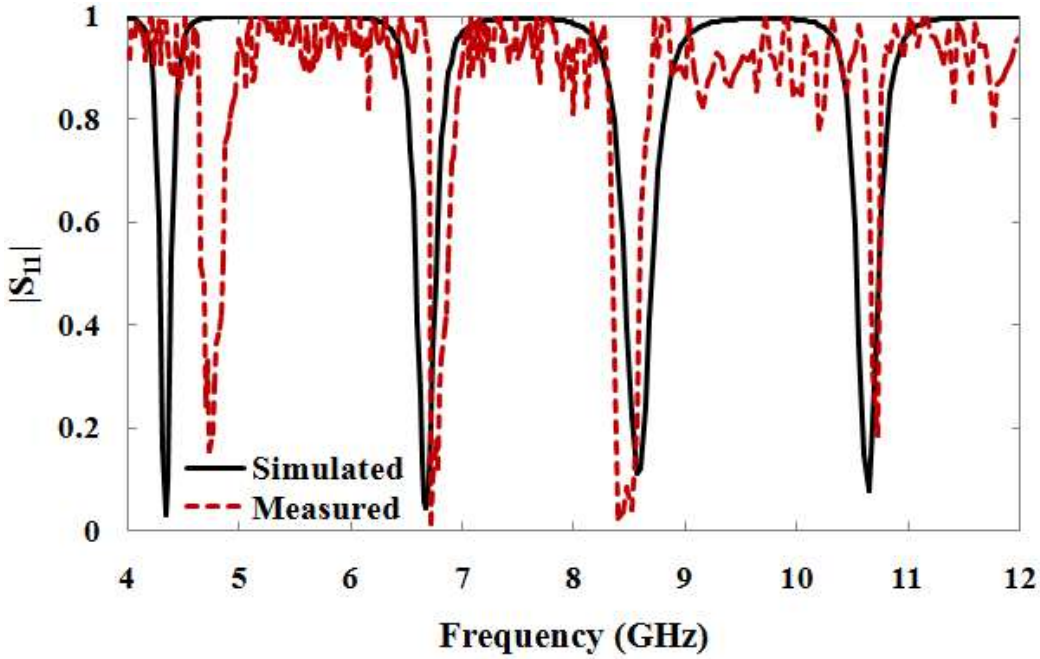

Figure 4.11: Comparison of simulated and measured reflection responses.

Table 4.2: Performance Comparison

Absorber	Absorption frequencies (GHz)	Relative Bandwidth	Unit cell periodicity	Thickness
[Zhang *et al.* (2013)]	6.69, 7.48, 8.67, and 9.91	6.88%, 6.82%, 6.00% and 4.44%	20 mm (0.446λ)	1.14 mm (0.0254λ)
[Mao *et al.* (2014)]	2.538, 7.092, 9.702, 13.302, and 15.588	Not Reported	20 mm (0.169λ)	1.5 mm (0.0127λ)
[Chaurasiya *et al.* (2015)]	3.91, 5.16, 7.10, and 9.16	Not Reported	23 mm (0.300λ)	1 mm (0.0130λ)
[Wang *et al.* (2015)c]	28.21, 39.59, 52.78, and 58.63	Not Reported	3.33 mm (0.313λ)	0.217 mm (0.0204λ)
Proposed	4.34, 6.68, 8.58, and 10.64	3.92%, 4.04%, 4.66%, and 2.91%	20 mm (0.289λ)	0.8 mm (0.0115λ)

where λ corresponds to the lowest peak absorption frequency.

4.7 Conclusion

An ultrathin quad-band metamaterial absorber has been presented in this chapter. The proposed structure has peak absorptivities in the C- and X-frequency bands. Resonators in a unit cell were oriented perpendicular to each other to design symmetrical unit cell. The four-fold symmetric structure provided polarization-insensitiveness. The proposed absorber has wide-angle performance. The absorption peaks can be tuned in the entire C- and X- band by changing the geometrical parameter. The *E*-field and surface current distributions on the proposed absorber unit cell have been studied for getting insight into the absorption mechanism. The measured result has been obtained by free space measurement method and found in good agreement with the simulated results.

A variant of the metasurface geometry presented in this chapter that is a patch enclosed in a CRR and connected to it at the diagonals is utilized to decouple antenna elements in a four-element MIMO antenna array in the next chapter. The metasurface utilized as an isolator is an asymmetric version of the present geometry to have dissimilar behavior for the TE and TM polarized incident wave.